Available online at www.sciencedirect.com

SCIENCE DIRECT®

Surface Science 560 (2004) 191–204

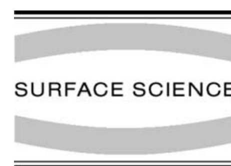

www.elsevier.com/locate/susc

Effects of methyl substitution on room-temperature chemisorption of *para*-xylene on Si(1 0 0)2×1 and modified surfaces: a thermal desorption and DFT study

Q. Li, Z.H. He, X.J. Zhou, X. Yang, K.T. Leung *

Department of Chemistry, University of Waterloo, Waterloo, Ont., Canada, N2L 3G1

Received 17 January 2004; accepted for publication 7 April 2004
Available online 11 May 2004

Abstract

The room-temperature (RT) adsorption and surface reactions of *para*-xylene (1,4-dimethylbenzene) on Si(1 0 0)2×1 have been investigated by thermal desorption spectrometry (TDS), low-energy electron diffraction (LEED), and Auger electron spectroscopy (AES). *p*-Xylene is found to adsorb on Si(1 0 0)2×1 at a saturation coverage of 0.30 monolayer without inducing discernible change to the 2×1 reconstruction. The chemisorption of *p*-xylene on the 2×1 surface primarily involves bonding through the phenyl group in a [4 + 2] cycloaddition configuration. Upon annealing, approximately 10% of the adspecies is found to desorb molecularly (at 350–500 K) while the majority remains on the surface after H abstraction from the methyl group (near 810 K). Condensation oligomerization of *p*-xylene has also been observed on Si(1 0 0)2×1 and could likely be enhanced upon irradiation by low-energy electrons. On sputtered and oxidized Si(1 0 0) surfaces, additional thermally induced fragmentation of the adsorbed *p*-xylene is found. Furthermore, large post-exposure of atomic hydrogen to the adsorbed *p*-xylene could not only lead to Si–C bond cleavage and the formation of alkane adspecies, but also play an important role in controlling various thermal reactions.
© 2004 Elsevier B.V. All rights reserved.

Keywords: Thermal desorption spectrometry; Chemisorption; Silicon; Aromatics; Molecule–solid reactions

1. Introduction

Molecular engineering of organic semiconductors has attracted a lot of recent attention because of their unique physical and electronic properties [1] and of their potential applications in the microelectronics industry [2–5]. Given that the physical and electronic structures of Si dimers on a Si(1 0 0)2×1 surface are generally similar to those of alkenes, studies of the interactions of organic molecules with Si(1 0 0) could provide useful insights into organosilicon chemistry, which help in the development of new strategies for functionalization of organic semiconductors and electronic devices [6].

The interaction of benzene with Si has been the subject of extensive experimental [7–12] and

* Corresponding author. Tel.: +1-519-888-4567x5826; fax: +1-519-746-0435.
E-mail address: tong@uwaterloo.ca (K.T. Leung).

0039-6028/$ - see front matter © 2004 Elsevier B.V. All rights reserved.
doi:10.1016/j.susc.2004.04.043

theoretical studies [13–18]. These studies show that chemisorption of this homocyclic aromatic compound on Si(1 0 0)2×1 may result in different bonding configurations, among which the main pathway follows the Diels-Alder (or [4 + 2]) cycloaddition mechanism, giving rise to a di-σ bonded cyclohexa-2,5-diene-1,4-diyl adspecies. The thermal chemistry of benzene and toluene (or methylbenzene) on Si(1 0 0) surface has been investigated in our early work [19]. The methyl group in toluene appears to introduce more reactivity and additional surface processes than benzene. The presence of two methyl groups in xylene (or dimethylbenzene) may also produce similar effects as those of toluene on Si(1 0 0). The relative positions of the two methyl groups on the benzene ring give rise to different isomers, which may in turn affect their surface chemistry and other properties. Using Fourier-transform infrared spectroscopy (FTIR), Coulter et al. observed the same bonding structures for methyl-substituted aromatic hydrocarbons (toluene and xylene) as benzene on Si(1 0 0), and further suggested that dissociation occurs predominantly via C–H bond cleavage of the methyl group after adsorption [20].

In the present work, the room-temperature adsorption, thermal desorption and other surface chemical processes of *p*-xylene on Si(1 0 0) have been investigated. Of the three xylene isomers: *p*-xylene (or 1,4-dimethylbenzene), *m*-xylene (or 1,3-dimethylbenzene) and *o*-xylene (or 1,2-dimethylbenzene), *p*-xylene represents the most symmetrical isomer with the two methyl groups farthest apart, which therefore provides a more appropriate platform for investigating the effect of methyl content when compared with benzene and toluene. The effects of the relative locations of the methyl groups on silicon surface chemistry will be the subject of future work. Both *p*-xylene-d_{10} and *p*-xylene-dimethyl-d_6 are used in the present experiment to investigate the selective reactivity of the phenyl and methyl groups on Si(1 0 0).

2. Experimental method

The experimental setup and procedure for the TDS studies have been described in details elsewhere [19]. Briefly, the experiments were conducted in a home-built dual-chamber ultrahigh vacuum (UHV) system, with a base pressure better than 5×10^{-11} Torr. A 12.5×3.5 mm^2 substrate was cut from a polished p-type B-doped Si(1 0 0) wafer (0.4 mm thick) with a resistivity of 0.0080–0.0095 Ω cm. A type-K thermocouple was used to monitor the temperature of the sample, and an AC current was applied to provide direct heating. A home-built temperature controller was used to generate linear temperature ramping at an adjustable heating rate, typically set at 2 K/s for the present TDS experiments.

Before introduction into the UHV chamber, the Si sample was pre-cleaned by using a typical RCA procedure [21] to remove light organic contamination and to provide a thin passivating oxide film [22]. After the bakeout, the sample was outgassed at 900 K for 20 h until the pressure recovered to below 2×10^{-10} Torr. The sample was then flash-annealed to 1500 K while carefully keeping the vacuum below 1×10^{-9} Torr. Unlike benzene, *p*-xylene was found to be more "sticky" on the Si surface. Any residual carbon left after annealing in the subsequent cleaning cycle would cause contamination of the surface if the surface were treated with a high-temperature flash-anneal (a procedure commonly employed in STM experiments). In order to prolong the use of the same sample (to be well over 50 TDS runs), the Si(1 0 0) sample was first treated with several cycles of sputtering and low-temperature anneal (below 850 K) before applying the flash-anneal to 1500 K. The cleanliness of the Si(1 0 0) surface was verified by AES with the near-surface C concentration below its detection limit (typically 5% for a retarding-field LEED optics) and by the presence of a sharp 2×1 LEED pattern.

The chemicals: *p*-xylene and *p*-xylene-d_{10} (99+ atom% D), and *p*-xylene-dimethyl-d_6 (98+% D purity) used in the present study were obtained commercially from Aldrich and Cambridge Isotope Laboratories, respectively. These chemicals were further purified by repeated freeze-pump-thaw cycles prior to use. Sample dosing was performed by back-filling the sample preparation chamber with a precision leak valve to an appropriate pressure, as monitored by an uncalibrated

ionization gauge. All exposures [in units of Langmuir (1 L = 10^{-6} Torr-second)] were performed at RT unless stated otherwise. It should be noted that the TDS profiles for normal and deuterated xylenes were found to be identical in our TDS experiments, indicating that isotopic effect is not important for the thermal desorption process.

3. Results and discussion

3.1. Molecular desorption

The adsorption of *p*-xylene on Si(1 0 0)2×1 at RT has been studied as a function of exposure by LEED and AES. Upon different exposures of *p*-xylene to the Si(1 0 0) surface at RT, only a slight increase in the background intensity was observed in the two-domain (2×1) LEED pattern characteristic of a clean Si(1 0 0) surface, which suggests that the dimer-row structure of the Si substrate is generally preserved after the adsorption of *p*-xylene. The peak-to-peak ratio of the C(*K L L*) Auger peak to that of the Si(*L V V*) Auger peak is used to indicate the relative C moiety on the surface. Fig. 1 shows this ratio as a function of RT exposure for *p*-xylene, toluene and benzene on Si(1 0 0)2×1. The data for each of the adsorbates was compared with first-order and second-order adsorption kinetics [23] and they are all found to follow the first-order kinetics, indicating a non-dissociative, i.e. molecular, chemisorption. The observed non-dissociative nature of the adsorption process for *p*-xylene, toluene and benzene therefore suggests that the adsorption of these aromatic molecules involves a common mechanism, likely via cycloaddition of the aromatic ring. For *p*-xylene, the ratio appears to reach its saturation value at 2 L exposure, which generally marks the completion of adsorption of the first monolayer (ML). The saturation coverage of benzene has been estimated to be 0.27 ML by Taguchi et al. [7]. From the ratio of the saturation values for relative surface C moiety of *p*-xylene (12%) and benzene (8.0%) and after taking into account the number of carbon atoms in *p*-xylene (8) and benzene (6), the saturation coverage for *p*-xylene is estimated to be 0.30 ML, which corresponds approximately to two

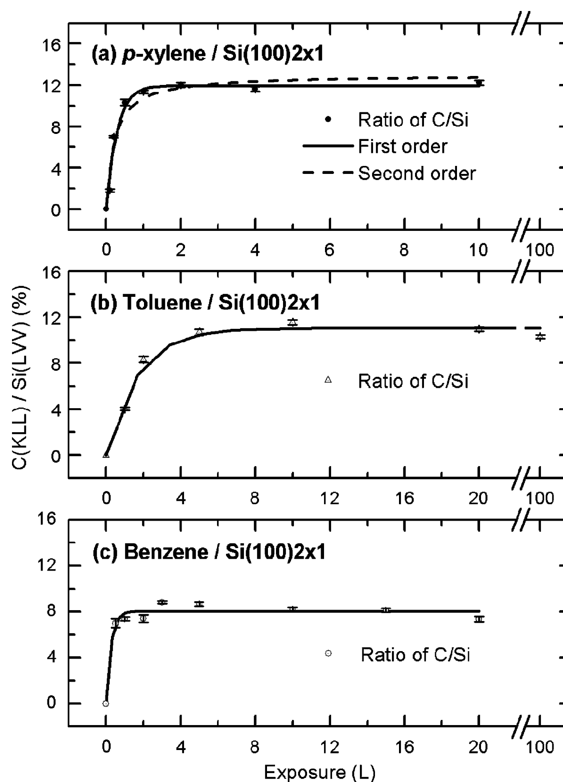

Fig. 1. Relative carbon moiety as indicated by the peak-to-peak intensity ratio for the C(*K L L*) to Si(*L V V*) Auger transitions as a function of room-temperature exposure of (a) *p*-xylene, (b) toluene and (c) benzene to Si(1 0 0)2×1. The experimental data are found to follow the first-order kinetics.

molecules for every three Si dimers on the 2×1 surface. It should be noted that the slightly higher value of the saturation coverage for *p*-xylene on Si(1 0 0)2×1 relative to that for benzene could be attributed to additional interaction due to one of its methyl groups with the Si surface. On the other hand, that this saturation coverage of *p*-xylene (0.30 ML) is lower than that of toluene on Si(1 0 0)2×1 (0.33 ML) could be the result of steric effects due to the presence of the second methyl group in *p*-xylene.

Fig. 2a shows the TDS profiles of mass 98 (base-ion mass) and mass 4 (D_2) for a 5-L RT exposure of *p*-xylene-d_{10} on Si(1 0 0)2×1. It should be noted that deuterated *p*-xylene was used in our TDS experiments in order to avoid the large H_2 background commonly found in stainless steel

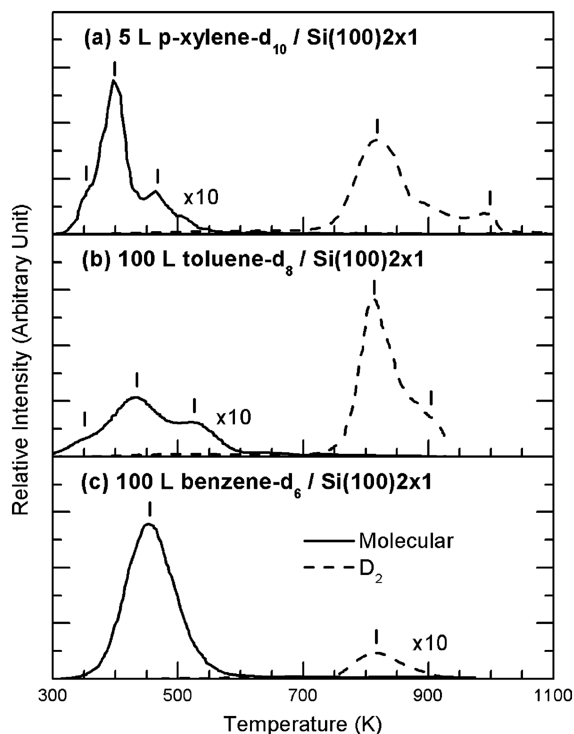

Fig. 2. Comparison of thermal desorption profiles of molecular (solid line) and mass-4 (D_2) desorption (dashed line) for saturation exposures of (a) *p*-xylene-d_{10}, (b) toluene-d_8, and (c) benzene-d_6 to Si(1 0 0)2×1 at room temperature.

UHV chambers [24]. In addition to the base-ion mass (mass 98, C_7D_7), the parent-ion mass (mass 116) and other ionic fragments including mass 110 (C_8D_7) and mass 82 (C_6D_5) were also monitored during the TDS experiments (not shown). Since their corresponding TDS peak intensities were found to follow the cracking pattern of *p*-xylene-d_{10} [25] over the same temperature range for the mass-98 profile, these ionic fragments could be attributed to dissociation of molecularly desorbed *p*-xylene-d_{10} in the ionizer of the quadrupole mass spectrometer (QMS). The TDS profile of mass 98 can therefore be used to indicate molecular desorption of *p*-xylene-d_{10} from Si(1 0 0)2×1. Evidently, two molecular desorption states with desorption maxima at 400 and 470 K for *p*-xylene-d_{10} are found to be similar in temperature to those of the corresponding primary molecular desorption from single-dimer geometry for toluene (at 430 K, Fig. 2b) and benzene (at 460 K, Fig. 2c) on Si(1 0 0)2×1 [7,19].

In order to understand the equilibrium geometries and enthalpy changes for different adsorption structures, we performed density functional theory (DFT) calculations for *p*-xylene interacting with a triple-dimer surface of a $Si_{21}H_{20}$ cluster used as a model for the Si(1 0 0)2×1 surface by using the Gaussian 98 program [26]. In particular, the hybrid functional consisting of Becke's 3-parameter non-local exchange functional and the correlation functional of Lee–Yang–Parr (B3LYP) was used along with the 6-31G(d) basis set [27]. Fig. 3 shows the optimized geometries for *p*-xylene/$Si_{21}H_{20}$ involving bonding through the phenyl group, which include the [4 + 2] cycloaddition structures of 2,5-dimethylcyclohexa-2,5-diene-1,4-diyl (Fig. 3a) and 1,4-dimethylcyclohexa-2,5-diene-1,4-diyl (Fig. 3b) adspecies, as well as the [2 + 2] cycloaddition structure of 3,6-dimethylcyclohexa-3,5-diene-1,2-diyl adspecies (Fig. 3c). The corresponding enthalpy changes with zero-point energy corrections, ΔE, are found to be −18.9, −10.9 and −5.5 kcal/mol, respectively. In our earlier work, we attributed the molecular desorption peak at 460 K of benzene/Si(1 0 0)2×1 to a [4 + 2] cycloaddition (cyclohexa-2,5-diene-1,4-diyl) adspecies (Fig. 4a), with $\Delta E = -16.7$ kcal/mol obtained by a similar DFT calculation for benzene/$Si_{21}H_{20}$ [19]. The similarity in ΔE to that of benzene/$Si_{21}H_{20}$ for both [4 + 2] cycloaddition adspecies (Fig. 3a and b) of *p*-xylene/$Si_{21}H_{20}$ found in the present DFT calculation suggests that the prominent molecular desorption features at 400 and 470 K can be similarly assigned to 1,4-dimethylcyclohexa-2,5-diene-1,4-diyl (Fig. 3b) adspecies and 2,5-dimethylcyclohexa-2,5-diene-1,4-diyl (Fig. 3a), respectively. The least stable [2 + 2] cycloaddition adspecies (Fig. 3c) could be attributed to the intensity at the lower desorption temperature of 350 K (Fig. 2a), which could be shown later to be related to adsorption on defect sites. It should be noted that all of these molecular adsorption structures only involve bonding between the phenyl group and the Si dimer, which is consistent with an earlier FTIR study reported by Coulter et al. [20]. Furthermore, the temperature difference for the desorption features of the [4 + 2] cycloaddition adspecies

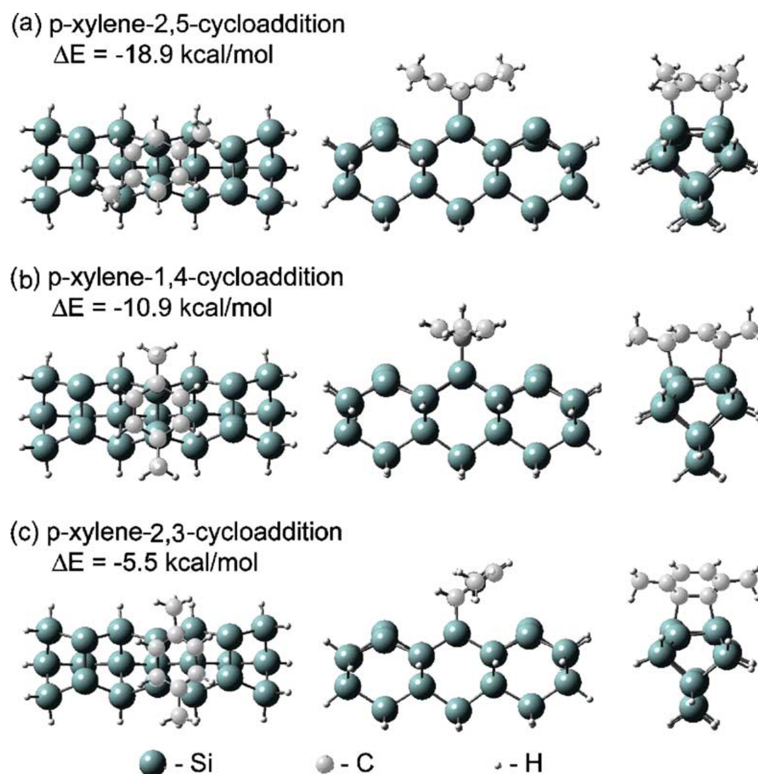

Fig. 3. Schematic diagrams of the adsorption geometries and the corresponding adsorption energies ΔE for (a,b) [4 + 2] cycloaddition and (c) [2 + 2] cycloaddition of *p*-xylene on a model surface of $Si_{21}H_{20}$, obtained by a density functional calculation with B3LYP/6-31G(d).

is evidently due to the relative positions of the methyl groups with respect to the C–Si bonding points.

In the case of benzene and toluene on Si(1 0 0), a more stable double-dimer adsorption geometry with the so-called "tight bridge" (TiB) configuration has been reported previously [11,16]. This adsorption configuration was believed to be converted from the initial "metastable" single-dimer [4 + 2] cycloaddition geometry upon chemisorption [11,16]. In the TDS profiles of benzene and toluene, the respective molecular desorption feature with desorption maximum in the range of 520–550 K has been attributed to the TiB state. By using the aforementioned DFT computational method, the corresponding enthalpy change of the TiB adsorption state of *p*-xylene on Si(1 0 0) is calculated to be −26.4 kcal/mol [compared to −18.9 kcal/mol (Fig. 3a) and −10.9 kcal/mol (Fig. 3b) for the single-dimer states]. These values are found to be on a similar relative scale as those for benzene/Si(1 0 0) [16] and toluene/Si(1 0 0) [28], which suggests a similar temperature range for the desorption maximum of *p*-xylene from the TiB state (520–550 K). However, the TiB state for benzene and toluene could only be clearly observed in the case of low coverage (<0.1 L) and was found not to be prominent at higher coverage in the earlier [19,29] and the present work (Fig. 2). Evidently, molecular desorption above 500 K for a saturation coverage of *p*-xylene/Si(1 0 0) is also found to be relatively weak (Fig. 2a), therefore suggesting that the TiB state does not predominate at high coverage. At high coverage, steric effects arising from the two methyl groups in *p*-xylene therefore appear to be more important in controlling the adsorption geometry. Furthermore, the unexpected higher saturation coverage for *p*-xylene/Si(1 0 0) than that for benzene/Si(1 0 0) as observed

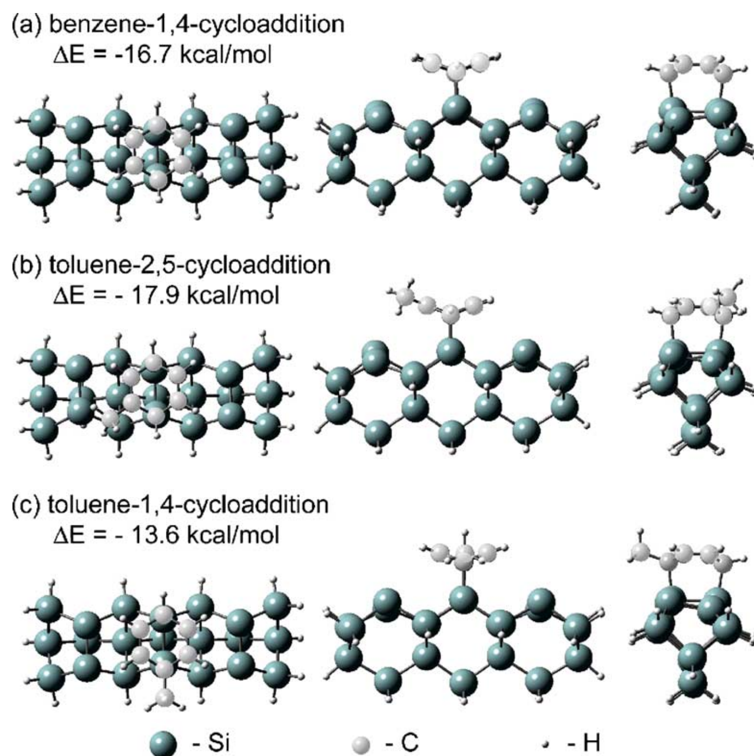

Fig. 4. Schematic diagrams of the adsorption geometries and the corresponding adsorption energies ΔE for [4 + 2] cycloaddition of (a) benzene and (b,c) toluene on a model surface of $Si_{21}H_{20}$, obtained by a density functional calculation with B3LYP/6-31G(d).

from our AES data (Fig. 1) is consistent with the lower relative population of the double-dimer adsorption geometry for *p*-xylene. Finally, as all of the TDS experiments were performed immediately after sample exposure in the present work, there would not be sufficient time for the single-dimer state to convert to the TiB state [11,16]. As such, while we acknowledge the plausible existence of the TiB state, we will not consider it further in the present work.

In order to investigate the influence of the methyl group on the [4 + 2] cycloaddition of aromatic hydrocarbons on Si(1 0 0), two adsorption geometries of toluene/$Si_{21}H_{20}$, 2-methylcyclohexa-2,5-diene-1,4-diyl (Fig. 4b) and 1-methylcyclohexa-2,5-diene-1,4-diyl (Fig. 4c), are also determined with a similar DFT calculation, and compared with that of benzene/$Si_{21}H_{20}$ as cyclohexa-2,5-diene-1,4-diyl adspecies (Fig. 4a). The adsorption enthalpy changes (ΔE) of toluene/$Si_{21}H_{20}$ with a methyl group attached to an ipso C (i.e., a C atom in the phenyl group that is attached to a substrate atom) and that to a non-ipso C are found to be 3.1 kcal/mol lower and 1.2 kcal/mol higher, respectively, than the enthalpy change of benzene/$Si_{21}H_{20}$. Furthermore, it is of interest that the enthalpy changes of *p*-xylene/$Si_{21}H_{20}$, with an additional methyl group attached to an ipso C and a non-ipso C, are found to be 2.7 kcal/mol lower and 1.0 kcal/mol higher, respectively, than that of toluene/$Si_{21}H_{20}$. Qualitatively, the enthalpy changes for the [4 + 2] cycloaddition of *p*-xylene on Si(1 0 0) can be used to infer the relative position of the methyl group(s) to the ipso C, and this picture is consistent with the TDS features shown in Fig. 2a.

3.2. Hydrogen evolution

In addition to the molecular desorption profile, the mass-4 (D_2) TDS profile for *p*-xylene-d_{10} on Si(1 0 0)2 × 1 is also shown in Fig. 2a and found to have a desorption maximum at 820 K, similar in

temperature to that of recombinative hydrogen desorption from Si monohydride (at 800 K) [30,31]. The slightly higher temperature of the desorption maximum from that of desorption from monohydride by 20 K [30,31] and the broad mass-4 profile extending to 1000 K (Fig. 2a) can be attributed to different H sources on the surface during the thermal desorption process. As observed in our previous TDS studies for toluene [19], pyridine [23] and styrene [32] on Si(1 0 0), hydrogen abstraction of *p*-xylene near or below its molecular desorption temperature could stabilize the adsorbate on Si(1 0 0) at higher temperature and further facilitate other reactions. For example, after H has been abstracted from a methyl group of *p*-xylene to the surface, the resulting radical would become more tightly bound to the surface through the methyl C (if the two strained σ bonds from the phenyl group are broken to yield a fully aromatic benzene ring). This hypothesis is also supported by earlier studies for acetylene on Si(1 0 0) [33,34]. In particular, similar TDS profiles for hydrogen desorption have also been obtained by Taylor et al. for the adsorption and decomposition of C_2H_2 on Si(1 0 0)2×1 [33]. Using high-resolution electron energy-loss spectroscopy, Huang et al. later found that the dissociation of adsorbed acetylene occurs via C–H bond breakage over a wide temperature range of 750–900 K, which evidently starts below the molecular desorption maximum of C_2H_2 at 760 K [34].

Fig. 2 also compares the TDS profiles of mass-4 (D_2) for a RT saturation exposure of *p*-xylene-d_{10} with those of toluene-d_8 and benzene-d_6 on Si(1 0 0)2×1, which show similar temperature values of the desorption maxima for all three molecules. Similar to those observed for the adsorption of toluene on Si(1 0 0)2×1 (Fig. 2b) [19], the intensity of D_2 desorption for *p*-xylene-d_{10} on Si(1 0 0)2×1 (Fig. 2a) is considerably higher (almost 10-fold) than that for the corresponding molecular desorption. However, the intensity of D_2 desorption for benzene-d_6 is significantly lower than that of molecular desorption (Fig. 2c), which clearly indicates that molecular desorption is the predominant process for benzene but not for its methyl-substituted derivatives. In addition, a weaker D_2 desorption feature is also observed for *p*-xylene-d_{10} and for toluene-d_8 with desorption maxima near 1000 and 900 K respectively, which further suggests the presence of an additional pathway for H evolution for these methyl-substituted benzene derivatives.

In order to determine whether the methyl group or the phenyl group is involved in the hydrogen abstraction process of *p*-xylene, the TDS profile of mass 4 for a 5 L exposure of *p*-xylene-dimethyl-d_6 (i.e., with just the methyl groups deuterated) is compared with that of a 5 L exposure of *p*-xylene-d_{10} (i.e. with both the phenyl and the methyl groups deuterated) to Si(1 0 0)2×1 at RT in Fig. 5. The two desorption profiles have been arbitrarily normalized at the peak maxima at 820 K. Evidently, the desorption of D_2 at 1000 K is only found in the TDS profile for *p*-xylene-d_{10} but not that for *p*-xylene-dimethyl-d_6 on Si(1 0 0)2×1. Hydrogen evolution originated from the methyl groups (*p*-xylene-dimethyl-d_6) could therefore occur only through surface-mediated abstraction followed by recombination desorption from monohydride sites at 820 K. Although the desorption intensity at 1000 K could only come from hydrogen evolution from the phenyl group, we cannot rule out any plausible contribution of the phenyl group to the TDS feature at 820 K. Indeed, the TDS profile of mass 3 (not shown), corresponding to recombinative desorption of methyl D and phenyl H, for *p*-xylene-dimethyl-d_6 has also been observed at 820 K.

The shape of the desorption feature at 820 K for *p*-xylene-dimethyl-d_6 on Si(1 0 0)2×1 can be understood by a pseudo second-order desorption kinetics model [35]. In particular, the kinetics of hydrogen evolution from the methyl group can be investigated using a simple lattice gas model similar to that for the H-terminated Si(1 0 0) surface proposed by D'Evelyn et al. [36]. In this model, there is only one desorption channel of H_2 resulting from monohydride (two H atoms paired on the same silicon dimer on Si(1 0 0)2×1), i.e.

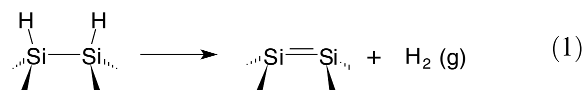

(1)

In the present case in which aromatic hydrocarbons (R) are involved, the distributions of species,

including doubly occupied dimers, are determined by two independent equilibria:

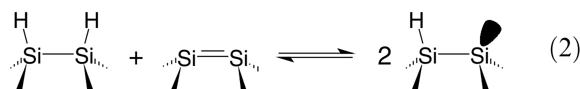

(2)

and

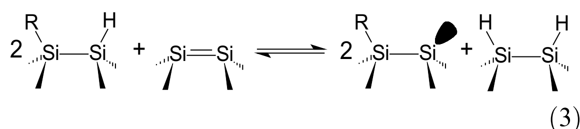

(3)

It is important to note that equilibria (2) and (3) are used only to define the distributions of species present on the surface, and they are not meant to be part of the mechanism by which these equilibrium distributions are established. The reaction enthalpy changes for equilibria (2) and (3) could be estimated by a DFT calculation similar to that used in Section 3.1 and were found to be +6.0 and +5.4 kcal/mol, respectively. The equilibrium concentration of monohydride on Si(1 0 0) can therefore be calculated for any given coverages of *p*-xylene and of overall surface hydrogen at a given temperature. The desorption rate of H_2 can then be obtained as:

$$r_d = -\frac{d\theta_H}{dt} = \theta_2 \cdot \nu \cdot e^{-E_d/RT} \quad (4)$$

where θ_H is the overall coverage of H atoms on the surface, θ_2 is the coverage of H atoms at the monohydride sites, ν and E_d are, respectively, the pre-exponential factor and activation energy for H_2 desorption. Fig. 5 shows that the experimental TDS profile for 5 L of *p*-xylene-methyl-d_6 can be effectively simulated using fitted parameters $\nu_d = 5.6 \times 10^{14}$ s^{-1} and $E_d = 53$ kcal/mol, which are found to be similar to the results obtained for H_2 desorption from monohydride [36]. From this numerical analysis, the desorption rate for H_2 is found to follow a near-second-order desorption kinetics with respect to the overall H coverage θ_H. The good accord between the experimental TDS profile of *p*-xylene-dimethyl-d_6 and the fitted profile shown in Fig. 5 therefore supports the hypothesis that hydrogen evolution from the methyl groups of *p*-xylene on Si(1 0 0)2×1 follows a near-second-order desorption kinetics. It should be noted that hydrogen evolution from monohydride sites on Si(1 0 0)2×1 follows a near-first-order desorption kinetics [36]. The presence of equilibrium (3) therefore could greatly affect the desorption kinetics of hydrogen evolution. In addition, the desorption feature at ~1000 K for the hydrogen evolution from the phenyl group could be the result of a condensation polymerization process that can be understood with a two-dimensional diffusion model in a "modified" collision theory, and this will be discussed in a later study [35].

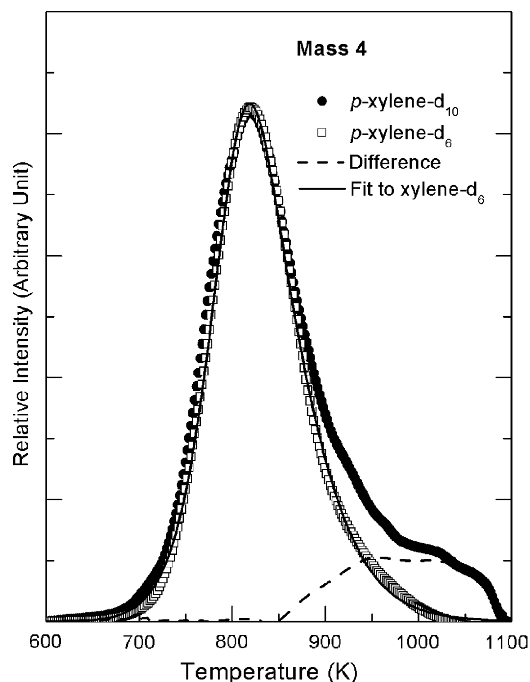

Fig. 5. Comparison of thermal desorption profiles of mass-4 (D_2) desorption for a 10 L exposure of *p*-xylene-d_{10} and that for a 10 L exposure of *p*-xylene-dimethyl-d_6, both to Si(1 0 0)2×1 at room temperature. The two data sets have been arbitrarily normalized at 820 K and the difference is shown by a dashed line. The experimental desorption data for *p*-xylene-d_6 has been fitted with a near-second-order desorption kinetics model (solid line) as discussed in the text.

3.3. Surface conditions study

Fig. 6 compares the TDS profiles for molecular desorption (mass 98) and desorption of dissociative products (mass 28 and mass 4) for a saturation

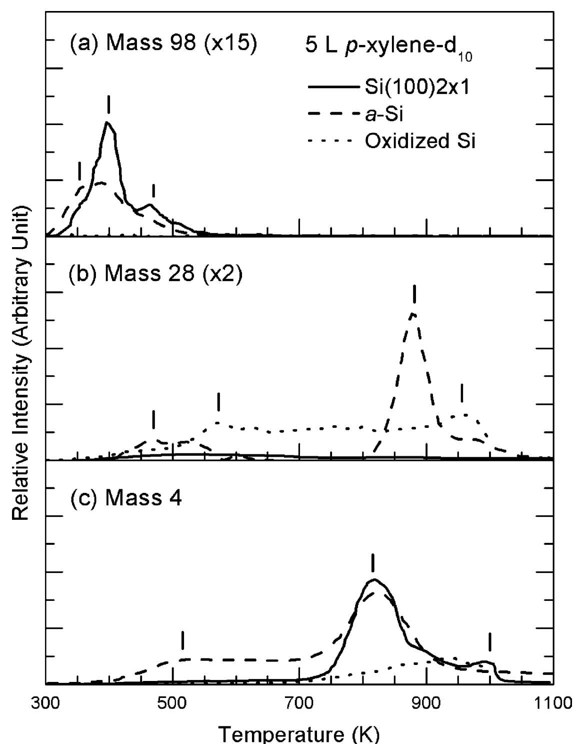

Fig. 6. Thermal desorption profiles for (a) mass 98 (molecular desorption), (b) mass 28 (dissociative products), and (c) mass 4 (D_2) for a 5 L exposure of *p*-xylene-d_{10} to Si(1 0 0)2×1 (solid lines), amorphous (a)-Si (dashed lines), and oxidized Si surface (dotted lines) at room temperature.

exposure (5 L) of *p*-xylene-d_{10} to a 2×1, amorphous and oxidized surfaces of Si(1 0 0) at RT. The amorphous surface (a-Si) was produced by ion sputtering in 4×10^{-5} Torr of Ar at 1 keV impact energy for 20 min, while the oxidized Si surface was obtained by exposing a clean 2×1 surface with 100 L of O_2 at RT. The lack of any long-range order for both a-Si and oxidized Si surfaces was confirmed by the absence of a LEED pattern.

In the TDS profiles of molecular desorption on a-Si (Fig. 6a), the desorption features at 400 and 470 K, both corresponding to [4 + 2] cycloaddition adspecies shown in Fig. 3b and a respectively, are found to be reduced in intensity relative to the corresponding features observed for the 2×1 surface. On the other hand, enhanced desorption intensity is observed for the feature at 350 K for a-Si, suggesting molecular desorption from defect sites likely involving the [2 + 2] cycloaddition adspecies shown in Fig. 3c. The enhancement of the low-temperature desorption feature on the sputtered surface is similar to that observed for toluene on a-Si [19]. In contrast to the weak and broad band of mass 28 for the 2×1 surface in the 400–800 K region, the desorption intensity in the same temperature region is found to increase noticeably for the sputtered surface, which suggests enhanced desorption of smaller fragments. Furthermore, as was previously observed for pyridine and styrene on a-Si, a strong mass-28 TDS feature at 880 K (Fig. 6b) is also found for *p*-xylene and can be attributed to dissociative desorption of larger hydrocarbon adspecies. Since a significant amount of mass-40 desorption was also observed at 880 K (not shown), which corresponds to desorption of ion-implanted Ar due to the sputtering process, this mass-28 TDS feature at 880 K could therefore be attributed to dissociative desorption of hydrocarbon fragments from a fairly active surface as a result of significant structural rearrangement accompanied with Ar desorption near 880 K. The shapes and desorption maxima of the TDS profiles of D_2 (mass 4, Fig. 6c) for a-Si are found to be generally similar to those observed on a Si(1 0 0)2×1 surface. The enhanced intensity observed in the lower-temperature region (400–700 K) for the sputtered surface is likely related to the desorption of smaller fragments found in the mass-28 TDS profile.

Fig. 6 also shows the TDS profiles of mass 98, mass 28 and mass 4 for a 5 L RT exposure of *p*-xylene-d_{10} to an oxidized Si surface. Evidently, significant reductions in molecular desorption (mass 98, Fig. 6a) and hydrogen evolution (mass 4, Fig. 6c) are found for the oxidized surface, which could be attributed to the loss of active adsorption sites due to oxidation. Furthermore, the discernible desorption features of mass 28 (along with mass 26 and mass 30, not shown) in the 450–700 K region depicted in Fig. 6b could be attributed to desorption of small hydrocarbons. However, the lack of corresponding mass-26 and mass-30 desorption intensities for the mass-28 feature near 960 K suggests that the latter intensity could be due to recombinative desorption of CO formed from surface C with O on the oxidized surface, as

was previously proposed for styrene on an oxidized Si surface [32]. The latter desorption channel for mass 28 is evidently accompanied by D_2 (mass 4) desorption in the same temperature region (Fig. 6c).

Finally, passivation of the active sites can also be achieved by H atoms as demonstrated in a separate TDS experiment for *p*-xylene-d_{10} on a H-terminated Si(1 0 0)1 × 1 surface, in which desorption of mass 98 (base mass of *p*-xylene-d_{10}), mass 28 and mass 4 is not observed (not shown). The lack of reactivity of a H-terminated Si(1 0 0) surface towards *p*-xylene-d_{10} is therefore similar to that found for benzene and toluene [19].

3.4. Surface-mediated reactions of p-xylene on Si(1 0 0)2 × 1 post-exposed to atomic H, molecular O_2 and low-energy electrons

In order to investigate the interaction of atomic hydrogen with *p*-xylene adsorbed on Si(1 0 0)2 × 1, the sample saturated with a 5 L exposure of *p*-xylene-d_{10} was post-exposed with H atoms generated from 3000 L of H_2 with a hot W filament positioned 2 cm away. Liquid nitrogen was used to maintain the sample near or below RT during the post-hydrogenation experiment. After the post-hydrogenation, the 2 × 1 LEED pattern for the *p*-xylene-d_{10}-saturated surface was found to revert back to a 1 × 1 pattern, indicating total de-reconstruction of the surface structure. Evidently, the TDS features for the molecular (mass 98) desorption are totally diminished upon post-hydrogenation (Fig. 7). The mass-30 TDS features in the 500–700 K region and the weaker feature at 750 K could be attributed to desorption of $C_2D_2H_2$. In particular, the lower-temperature mass-30 TDS features along with the weaker mass-28 and mass-2 desorption features at 510 K are typical of molecular desorption of ethylene [37,38]. On the other hand, the unusually strong mass-28 TDS feature at 710 K relative to the mass-30 feature could be attributed to an additional pathway of dehydrogenation desorption of ethyl adspecies on a H-terminated Si(1 0 0) surface [32,39], indicating that post-hydrogenation could enhance the dissociation of the adsorbate as a result of bond saturation. The two mass-30 features at 630 and 750 K

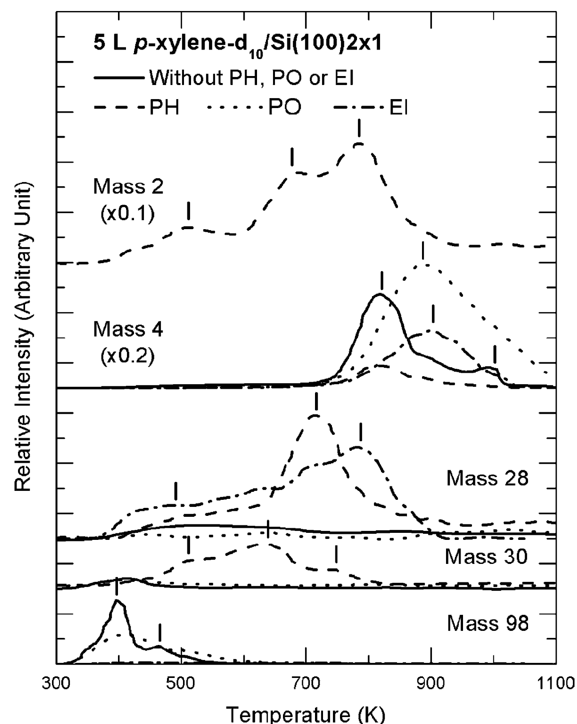

Fig. 7. Comparison of thermal desorption profiles of mass 2, 4, 28, 30, and 98 for a 100 L room-temperature exposure of *p*-xylene-d_{10} to Si(1 0 0)2 × 1 (solid lines), and with post-hydrogenation (PH, dashed lines), post-oxidation (PO, dotted lines), and post-electron-irradiation (EI, dashed-dotted lines) at 200 μA and 80 eV for 30 min.

can be attributed to ethylene evolution from two separated H-terminated Si(1 0 0) phases (dihydride and alternating dihydride–monohydride) in surface-mediated processes driven by thermal diffusion and desorption of hydrogen [32]. In addition, the two intense TDS features of mass 2 at 680 and 790 K for the post-hydrogenated sample could be assigned to recombinative desorption from dihydride and monohydride, respectively, on a H-terminated Si(1 0 0) surface [30,31]. At 820 K, the mass-4 desorption from the post-hydrogenated sample is found to be greatly reduced while the corresponding mass-3 desorption is evidently similar to that from the 2 × 1 surface at 820 K (not shown), which suggests strong recombinative desorption involving post-adsorbed H atoms and D atoms from the *p*-xylene-d_{10} adspecies.

Fig. 7 also shows the TDS profiles for 5 L of *p*-xylene-d_{10} on Si(1 0 0)2×1 post-exposed with 100 L of O_2 at RT. As in the case of toluene and benzene [19], post-oxidation appears to partially reduce molecular (mass 98) desorption of *p*-xylene-d_{10}, which indicates the presence of surface-mediated interactions of oxygen with *p*-xylene-d_{10}. Furthermore, the mass-4 (D_2) evolution for *p*-xylene-d_{10}/Si(1 0 0)2×1 upon post-oxidation is found to be broadened and shifted to a higher temperature (from 820 to 890 K). Similar results have been reported and discussed in our earlier TDS studies on benzene and toluene [19], and they could be similarly attributed to be the result of surface-mediated oxidization of xylene. Similar to that on the Si(1 0 0)2×1 surface, the desorption intensities of mass 28 and mass 30 for the post-oxidized sample are found to be very weak, suggesting that post-oxidation will not help in producing fragments of adsorbed *p*-xylene.

Fig. 7 depicts the effects of low-energy electron irradiation on the TDS profiles of mass 98 (base mass), mass 28 and mass 4 for 5 L RT exposure of *p*-xylene-d_{10} to Si(1 0 0)2×1. Electron irradiation was performed on the Si sample (held at 80 V bias potential) for 30 min at 0.2 mA with electrons thermionically emitted from a hot W filament positioned 5 cm away. Evidently, electron irradiation greatly diminishes molecular desorption, which is likely due to electron-induced desorption [40] and/or conversion to other smaller dissociated or larger oligomerized adspecies. The TDS profile of mass 28 shows a marked increase in the desorption of dissociated fragments C_2D_2 (arising from molecular desorption of C_2D_2 or further dissociation of C_2D_4) caused by electron-induced dissociation of the adsorbed *p*-xylene-d_{10}. In particular, two enhanced desorption features of mass 28 are observed, with a maximum at 790 K and with a broad structure in the region of 400–700 K. Because molecular desorption of smaller hydrocarbons such as C_2H_4 on Si(1 0 0)2×1 generally occurs near 550 K [37,38], the broad mass-28 TDS feature in the region of 400–700 K can be attributed to the cracking patterns of desorbed fragments caused by electron irradiation. The mass-28 desorption feature at 790 K can be assigned to molecular desorption of acetylene (arising from electron dissociation), which has been reported to exhibit a desorption maximum at 690–740 K from Si(1 0 0)2×1 [33]. In addition, the intensity for the mass-4 TDS profile for the electron-irradiated sample appears to have been reduced by half relative to that for the 2×1 surface with its desorption maximum shifted from 820 to 900 K. The reduction in the relative intensity of the mass-4 TDS profile could be due to reduced moiety of hydrocarbons as a result of desorption of these fragments at a lower temperature. The increase in the temperature of the desorption maximum found in the present case has also been observed in our previous studies on electron irradiation of pyridine [23] and styrene on Si(1 0 0) [32]. Such an increase can also be similarly explained by a proposed mechanism involving electron-induced oligomerization of the adsorbate [23,32,35].

4. Concluding remarks

The RT adsorption and thermal reactions of *p*-xylene on Si(1 0 0)2×1 and related sputtered and oxidized surfaces have been investigated by using TDS, AES and LEED. *p*-Xylene is found to adsorb on the Si(1 0 0)2×1 surface predominantly through [4 + 2] cycloaddition and to have little effect on the two domain (2×1) long-range order of the Si(1 0 0) surface. The saturation coverage at RT is estimated to be 0.30 ML, in between that of benzene (0.27 ML) and toluene (0.33 ML), which illustrates the interplay between the effect of methyl substitution in enhancement and that of steric hindrance on chemisorption. Upon annealing, the adsorbate is found to desorb in part molecularly with desorption states at 400 and 470 K (from two different [4 + 2] cycloaddition geometries), while the majority of the adsorbate remains on the surface after hydrogen abstraction from the methyl group. Two hydrogen evolution states are observed at 820 and 1000 K, with the former involving H atoms abstracted from the methyl group followed by recombinative desorption of H_2 from the monohydride sites, and the latter involving H atoms released from the phenyl group as H_2 during condensation polymerization.

The sputtered Si surface exhibits additional adsorption that leads to molecular desorption at 350 K, and potentially opens up new reaction pathways for decomposition into acetylene (as shown in the mass-28 TDS profile at 880 K). On the other hand, considerably reduced molecular desorption and diminished hydrogen evolution on the oxidized Si surface are observed, due to oxygen passivation of the available active sites. Other processes such as CO production and/or condensation polymerization near 1000 K are found to be plausible on post-oxidized Si(1 0 0)2×1 surface saturated with *p*-xylene. Furthermore, a saturation exposure of atomic H is also found to totally passivate the Si(1 0 0)2×1 surface, producing a 1×1 surface that is inert to *p*-xylene adsorption. High post-exposure of atomic hydrogen, on the other hand, appears to saturate some of the double bonds of the adsorbed *p*-xylene on Si(1 0 0) that lead to further evolution of ethyl, ethylene and acetylene adspecies and a 1×1 structure. Moreover, dehydrogenation, diffusion and desorption of surface hydrogen appear to lead to more surface-mediated processes upon annealing.

Finally, preliminary studies on the adsorption of other xylene isomers, including *m*-xylene (1,3-dimethylbenzene) and *o*-xylene (1,2-dimethylbenzene) on Si(1 0 0)2×1 have also been performed.

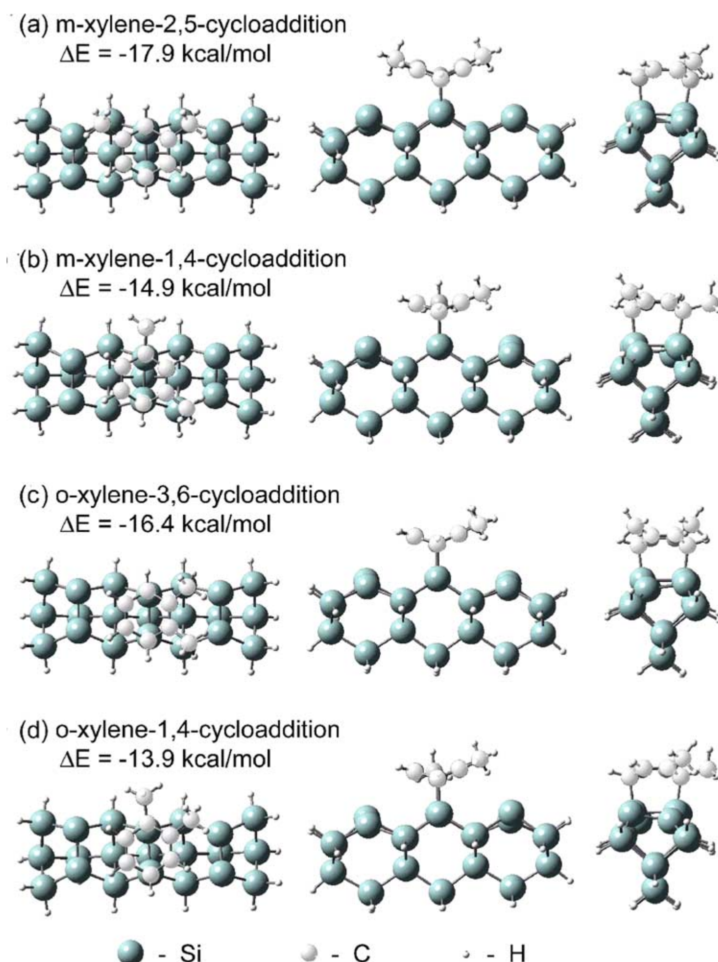

Fig. 8. Schematic diagrams of the adsorption geometries and the corresponding adsorption energies ΔE for [4 + 2] cycloaddition of (a,b) *m*-xylene and (c,d) *o*-xylene on a model surface of $Si_{21}H_{20}$, obtained by a density functional calculation with B3LYP/6-31G(d).

Fig. 8 compares the adsorption geometries and corresponding enthalpy changes ΔE of the [4+2] cycloaddition adspecies of *m*-xylene and *o*-xylene on Si(1 0 0)2×1. Similar to the results found for the adsorption of *p*-xylene and toluene, the adsorption structure with a methyl group attached to an ipso C is less stable than that without any methyl group attached to an ipso C. For example, ΔE for 1,4-dimethylcyclohexa-2,5-diene-1,4-diyl (−14.9 kcal/mol, Fig. 8b) is less negative than that for 2,6-dimethylcyclohexa-2,5-diene-1,4-diyl (−17.9 kcal/mol, Fig. 8a). Similarly, ΔE for 1,2-dimethylcyclohexa-2,5-diene-1,4-diyl (−13.9 kcal/mol, Fig. 8d) is less negative than that for 2,3-dimethylcyclohexa-2,5-diene-1,4-diyl (−16.4 kcal/mol, Fig. 8c). The differences of enthalpy changes between the ipso-C and non-ipso-C types of adsorption structures are 8.0, 3.0 and 2.5 kcal/mol for *p*-xylene, *m*-xylene and *o*-xylene, respectively. The larger difference for *p*-xylene relative to those for *m*-xylene and *o*-xylene is likely due to the attachment of two methyl groups to two ipso C atoms. It would be of great interest to conduct further surface analysis experiments (including TDS) to obtain more insights into the intricate adsorption structures and thermal chemistry of these xylene isomers on Si(1 0 0) and related surfaces.

Acknowledgements

This work was supported by the Natural Sciences and Engineering Research Council of Canada. It is our pleasure to acknowledge useful discussions with Professor Michael Chong.

References

[1] J.L. Reddinger, J.R. Reynolds, Adv. Poly. Sci. 145 (1999) 57.
[2] A. Tsumura, H. Koezuka, T. Ando, Appl. Phys. Lett. 49 (1986) 1210.
[3] A. Garito, R.F. Shi, M. Wu, Phys. Today 47 (1994) 51.
[4] J.R. Ostrick, A. Dodabalapur, L. Torsi, A.J. Lovinger, E.W. Kwock, T.M. Miller, M. Galvin, M. Berggren, H.E. Katz, J. Appl. Phys. 81 (1997) 6804.
[5] C. Joachim, J.K. Gimzewski, A. Aviram, Nature 408 (2000) 541.
[6] S.F. Bent, Surf. Sci. 500 (2002) 879.
[7] Y. Taguchi, M. Fujisawa, T. Takaoka, T. Okada, M. Nishijima, J. Chem. Phys. 95 (1991) 6870.
[8] Y. Taguchi, Y. Ohta, T. Katsumi, K. Ichikawa, O. Aita, J. Electron Spectrosc. Relat. Phenom. 88–91 (1998) 671.
[9] S. Gokhale, P. Trischberger, D. Menzel, W. Widdra, H. Droge, H.-P. Steinruck, U. Birkenheuer, U. Gutdeutsch, N. Rosch, J. Chem. Phys. 108 (1998) 5554.
[10] M.J. Kong, A.V. Teplyakov, J.G. Lyubovitsky, S.F. Bent, Surf. Sci. 411 (1998) 286.
[11] G.P. Lopinski, T.M. Fortier, D.J. Moffatt, R.A. Wolkow, J. Vac. Sci. Technol. A 16 (1998) 1037.
[12] B. Borovsky, M. Krueger, E. Ganz, Phys. Rev. B 57 (1998) R4269.
[13] B.I. Craig, Surf. Sci. 280 (1993) L279.
[14] H.D. Jeong, S. Ryu, Y.S. Lee, S. Kim, Surf. Sci. 344 (1995) L1226.
[15] U. Birkenheuer, U. Gutdeutsch, N. Rosch, Surf. Sci. 409 (1998) 213.
[16] R.A. Wolkow, G.P. Lopinski, D.J. Moffatt, Surf. Sci. 416 (1998) L1107.
[17] P.L. Silvestrelli, F. Ancilotto, F. Toigo, Phys. Rev. B 62 (2000) 1596.
[18] X. Lu, M.C. Lin, X. Xu, N. Wang, Q. Zhang, Phys. Chem. Comm. 13 (2001) 1.
[19] Q. Li, K.T. Leung, Surf. Sci. 479 (2001) 69.
[20] S.K. Coulter, J.S. Hovis, M.D. Ellison, R.J. Hamers, J. Vac. Sci. Technol. A 18 (2000) 1965.
[21] W. Kern, D.A. Puotinen, RCA Rev. 31 (1970) 187.
[22] R.E. Novak, Solid State Technol. 31 (1988) 39.
[23] Q. Li, K.T. Leung, Surf. Sci. 541 (2003) 111.
[24] J.-P. Bacher, C. Benvenuti, P. Chiggiato, M.-P. Reinert, S. Sgobba, A.-M. Brass, J. Vac. Sci. Technol. A 21 (2003) 167.
[25] NIST/EPA/NIH Mass Spectral Library, NIST'98 with Windows, Version 1.7, 1996.
[26] Gaussian 98 (Revision A.11.3), M.J. Frisch et al., Gaussian Inc., Pittsburgh, PA, 2002.
[27] J.B. Foresman, Æ. Frisch, Exploring Chemistry with Electronic Structure Methods, second ed., Gaussian Inc., Pittsburgh, 1996, and references therein.
[28] F. Costanzo, C. Sbraccia, P.L. Silvestrelli, F. Ancilotto, J. Phys. Chem. B 107 (2003) 10209.
[29] B. Borovsky, M. Krueger, E. Ganz, J. Vac. Sci. Technol. B 17 (1999) 7.
[30] M. Suemitsu, H. Nakazawa, N. Miyamoto, Appl. Surf. Sci. 82/83 (1994) 449.
[31] S.M. Gates, R.R. Kunz, C.M. Greenlief, Surf. Sci. 207 (1989) 364.
[32] Q. Li, K.T. Leung, Surf. Sci., submitted for publication.
[33] P.A. Taylor, R.M. Wallace, C.C. Cheng, W.H. Weinberg, M.J. Dresser, W.J. Choyke, J.T. Yates Jr., J. Am. Chem. Soc. 114 (1992) 6754.
[34] C. Huang, W. Widdra, X.S. Wang, W.H. Weinberg, J. Vac. Sci. Technol. A 11 (1993) 2550.
[35] Q. Li, Ph.D. Thesis, University of Waterloo, Ontario, Canada (2004).
[36] M.P. D'Evelyn, Y.L. Yang, L.F. Sutcu, J. Chem. Phys. 96 (1992) 852.

[37] C.C. Cheng, W.J. Choyke, J.T. Yates Jr., Surf. Sci. 231 (1990) 289.
[38] L. Clemen, R.M. Wallace, P.A. Taylor, M.J. Dresser, W.J. Choyke, W.H. Weinberg, J.T. Yates Jr., Surf. Sci. 268 (1992) 205.
[39] W. Widdra, C. Huang, S.I. Yi, W.H. Weinberg, J. Chem. Phys. 105 (1996) 5605.
[40] V.N. Ageev, Prog. Surf. Sci. 47 (1994) 55, and references therein.